RESEARCHERID
THOMSON REUTERS

[NC-Rase 18]
DOI: 10.5281/zenodo.1495055

ISSN 2348 – 8034
Impact Factor- 5.070

GLOBAL JOURNAL OF ENGINEERING SCIENCE AND RESEARCHES

PREPARATION AND CHARACTERIZATION OF NANOCRYSTALLINE BI2O3: A NOVEL CANDIDATE FOR ETHANOL SENSING

Dr. S. D. KAPSE
Department of Physics, G. S. College, Khamgaon 444303, Maharashtra, India

ABSTRACT

The present paper describes synthesis and analysis of nanocrystalline powders of Bismuth oxide (Bi_2O_3) for etanol gas sensing application. The Bi_2O_3 were prepared by ethyl alcohol mediated decomposition route. The structural, electrical and reducing gas sensing properties of prepared samples was investigated. X-ray diffraction (XRD) was used to confirm the material structure and transmission electron microscopy (TEM) to depict the crystallite microstructure. The gas sensing properties of (Bi_2O_3) were studied by depositing thick films. Conductance responses of the nanocrystalline Bi_2O_3 based thick films were measured by exposing the film to reducing gases like ammonia (NH_3), liquefied petroleum (LPG), hydrogen sulfide (H_2S), and ethanol gas (C_2H_5OH). It was found that the sensor exhibited various sensing responses to these gases at different operating temperatures. No cross sensitivity was observed during the gas sensing measurements. Furthermore, fast response and good recovery are the main features of investigated sensors.

In order to continue the scaling trend there is need of solutions for issues occurred during the process integration. Thus there is increase in demand of new process technology and materials which should be coming up with new process. The reliability challenges for copper interconnects are discussed in present paper. Also need of low-k and porous low-k related issues are highlighted in this paper.

Keywords: *Bismuth oxide; Ethanol gas; Dopant; Response time*

I. INTRODUCTION

Over the last two decades, Bi_2O_3 has been investigated widely because of its structural, optical and electrical properties such as large band gap, refractive index, dielectric permittivity. In addition to this Bi_2O_3 have a remarkable photoconductivity and photoluminescence. The main attractive property of bismuth-based sensors is the low toxicity. Due these novel properties Bi_2O_3 has emerge as a promising material for including catalysts, electrical ceramics, solid-state electrolytes, gas sensors, superconductors, and so forth due to their particular electrical, optical and fast-ion conducting characteristics [1-11]. It has long been known that the electrical properties of a semiconducting material change as a result of adsorption and/or reaction with the gases in the atmosphere. This property of semiconducting materials is typically exploited in gas sensing measurements. Semiconducting oxides such as ZnO, TiO_2, Fe_2O_3, WO_3, and SnO_2 are commonly investigated materials for gas sensing applications.

Bismuth oxide (Bi_2O_3), which is usually taken as model for p-type semiconduction, has a wide range of pplications due to its good chemical stability as well as for its excellent optical and electrical properties. Bi_2O_3 is an important metal-oxide semiconductor with a direct band gap 2.85 and 2.58 eV for the monoclinic α- Bi_2O_3 and tetragonal β-Bi_2O_3 phases, respectively [12,13]. Bi_2O_3 appears in four polymorphic modifications denoted as α-, β-, γ - and δ-Bi_2O_3 [14-16]. All modifications are structurally characterized and their powder diffraction patterns have been discussed [17-23]. Nanocrystalline particles generally display properties different from their bulk counterparts from which they are derived. From literature survey it is observed that the gas sensing properties depend naturally on the catalytic or surface chemical properties of sensing materials used, beside their physical or morphological properties such as grain size, porosity and thickness[17,18]. Many chemical methods have been employed to prepare Bi_2O_3 nanoparticles, e.g. precipitation[17, 19], flame spray pyrolysis[20], and sol–gel methods [21-24]. From literature survey it is observed that, there are almost no reports on ethanol sensing properties of pure Bi_2O_3. Therefore present paper concentrate on synthesis of nanocrystalline Bi_2O_3 by thermal decomposition route in the aqueous medium of

[NC-Rase 18] ISSN 2348 – 8034
DOI: 10.5281/zenodo.1495055 Impact Factor- 5.070
ethyl alcohol. Further, structural, morphological, electrical and ethanol gas sensing properties of Bi_2O_3 have been investigated in details.

II. EXPERIMENTAL

II (a) Synthesis of nanocrystalline pure Bi_2O_3 power

Appropriate quantity of bismuth nitrate [Bi (NO_3) $3{\cdot}H_2O$] was grounded for 30 min. in an agate mortar pestle and then mixed with absolute ethanol. The mixture was vigorously stirred for ~2 hours at 70 ^{0}C temperature and then the suspension was transferred into a Teflon lined stainless steel autoclave. The temperature of the autoclave was raised slowly to 170 ^{0}C and maintained for 10 h. Thereafter, the autoclave was allowed to cool naturally to room temperature and the resulting product washed several times with deionized water and absolute ethanol to remove the possible residue. Then the product was kept for drying overnight at 100 ^{0}C in an oven, which was followed by calcination at 600 ^{0}C and for 6 h. It provides stricter standardization control of the documents. In other words, a template is a form or pattern used as a guide to making something. Due to it you do not need set the margins, spacing, page layout, fonts, format options, etc. every time.

II (b) Characterization of pure BI_2O_3 powders

The crystal phases of calcined samples were analyzed using X-ray diffraction (XRD), (Model: Philips X'pert) with copper target, Kα radiation (λ = 1.54059 Å). The average crystallite size has been calculated from the XRD peaks using Debye-Scherrer formula, provided in equation (1).

$$D = \frac{K\lambda}{B.Cos\theta} \quad \text{.....(1)}$$

Where B is the full width at half-maximum intensity (in radians) of a peak at an angle θ; K is a constant, depending on the line shape profile; λ is the wavelength of the X-ray source. The morphologies of the synthesized powder were observed through a transmission electron microscopy (TEM), (Model: Philips CM 200). Further the chemical bonding of structure were investigated by using Magna 560 FT-IR spectrometer with a KBr disk.

II(C) Measurement of gas sensing characteristics

For gas sensing properties, the calcined materials were grounded into fine powders, sieved and dispersed with a temporary binder as a mixture of organic solvents to form pastes. The ratio of inorganic to organic part was kept as 75:25 in formulating the paste. The paste was then used to prepare thick films. The thixotropic paste was screen printed on a glass substrate in desired patterns. The films prepared were fired at 500 ^{0}C for 2 h. Silver contacts were made by vacuum evaporation for electrical measurements. The thicknesses of the films were observed to be in the range from 25 to 30 μm. The reproducibility of the film thickness was achieved by maintaining the proper rheology and thixotropy of the paste.

The sensing performance of the sensors was examined using a 'static gas-sensing system'. The description of the schematic sensor assembly and the circuitry for the sensor characteristics measurement was reported in our earlier publication [25]. The time taken for the sensor to attain the maximum (90%) change in conductance on exposure to the target gas is measured as the response time. The time taken by the sensor to get back 90% of the original conductance is measured as the recovery time.

ISSN 2348 – 8034
Impact Factor- 5.070

III. RESULT AND DISCUSSION

III (a) Material Characterization

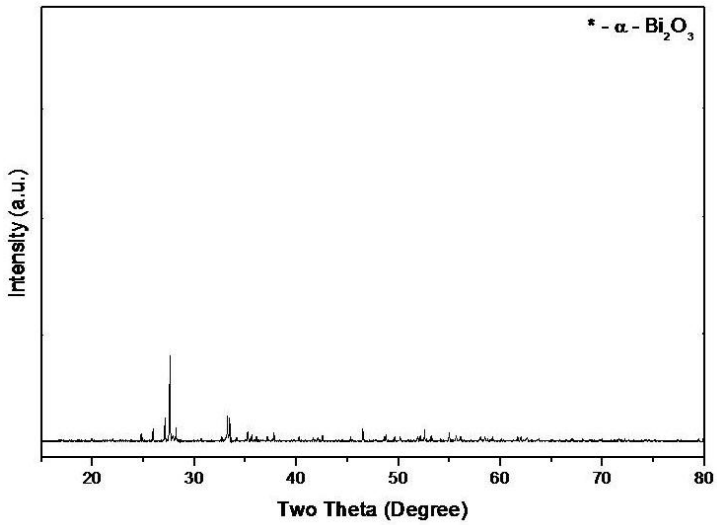

Fig. 1: XRD patterns of (a) pure Bi_2O_3 calcinated at 600 ^{0}C.

Bismuth oxide exists as two stable forms (monoclinic α -Bi_2O_3 and cubic-Bi_2O_3) and two other metastable phases (tetragonal β -Bi2O3 and bcc γ-Bi_2O_3), which can be converted to each other at certain condition [17]. In all cases, the forms strongly depend on the synthesis method. In our case, the XRD pattern (Fig. 1) of pure Bi_2O_3, calcinated at 600^{0}C and for 6 h, indicates that the powder has a high degree of crystallinity as shown by the highly intense and sharp peaks. In Fig. 1, all diffraction peaks are assigned to bismite crystallized in monoclinic form (α-Bi_2O_3) corresponding to JCPDS Card No. 01-072-0398. For the pure Bi_2O_3, only α- Bi_2O_3 phase was detected after cooling down to room temperature. Along with monoclinic form the traces of non-stiochiometric $Bi_2O_{2.33}$ phases are also seen.

The crystallite sizes were calculated by using Debye–Scherrer equation. The crystalline pattern of powders and the observed d-lines match the reported values for α-Bi_2O_3 phase. The calculated lattice parameters by least squares method are in good agreement with literature data reported for α - Bi_2O_3 phase, which also confirm that the synthesized powders are monoclinic Bi_2O_3 nanocrystallites.

The TEM image along with selected area electron diffraction (SAED) pattern of the pure Bi_2O_3 powder samples is depicted in Fig. 2. The TEM images of the pure powder samples depicted in shows that Bi_2O_3 nanoparticles are well dispersed and irregular in shape without evident agglomeration. The particles are of spherical in shape and the average particle size varies from 10 nm to 23 nm, which is in good agreement with the XRD result. The well defined SEAD pattern clearly shows the diffraction spots representing different lattice planes of α-Bi_2O_3.

ISSN 2348 – 8034
Impact Factor- 5.070

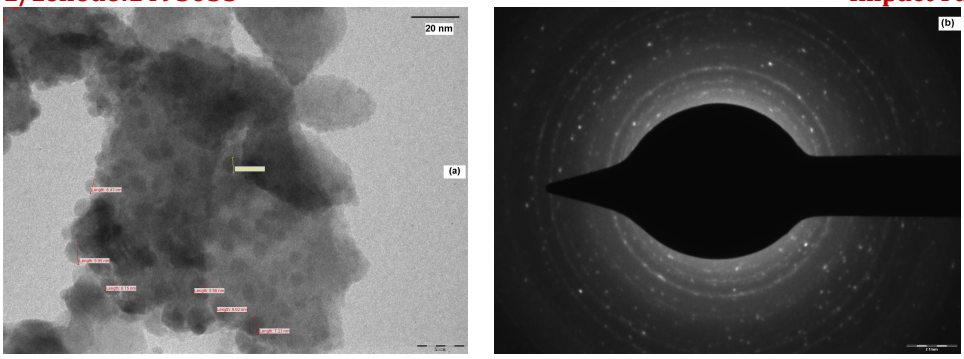

Fig. 2: a) TEM image and (b) selected area diffraction pattern of pure Bi_2O_3

FT-IR spectroscopy was useful technique to corroborate the results concerning the identification of the bismuth oxide phases given by the XRD pattern. The IR spectra of the Bi_2O_3 samples calcinated at 600 ^{0}C are depicted in Fig. 3. The spectra displayed a strong absorption band in the 544.00–443.00 cm^{-1} range is due to Bi–O stretching and deformation modes [26]. In the present investigations, the absorption band at about 443.00, 509.00 and 543.00 cm^{-1} in FTIR spectra can be assigned to α-Bi_2O_3 [27].

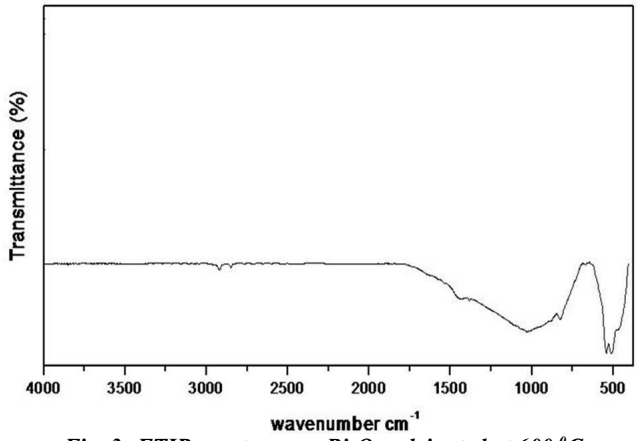

Fig. 3: FTIR spectra pure Bi_2O_3 calcinated at 600 ^{0}C

These findings are in agreement with XRD diffractogram results. Thus, pure Bi_2O_3 solid solution within the concentration investigated in this study can be obtained by ethanol mediated decomposition route. Besides, it needs to mention that an absorption band at about 1060 cm^{-1} is also observed. As organic molecules are removed completely, this absorption band may be attributed to the other kinds of vibrations of Bi–O caused by the interaction between the Bi–O bonds and their other surroundings [28].

III (D) Gas sensing studies of nanocrystalline pure BI_2O_3

The variation of response of pure Bi_2O_3 based sensor element as a function of operating temperature towards H_2, NH_3, CO_2, H_2S, LPG and ethanol is illustrated in Fig. 4. From figure it can be seen that the sensor response for each test gas increases with increase in operating temperature, reaches maximum corresponding to optimum operating temperature and decreases further. The response of a semiconductor oxide gas sensor to the given gas depends on the speed of the chemical reaction on the surface of the grains and the speed of diffusion of the gas molecules into the surface. These are the activation processes [26]. At low temperatures, the sensor response is restricted by the speed of the chemical reaction and at higher temperature it is restricted by the speed of diffusion of gas molecules. At some intermediate temperature, the speed of the two processes becomes equal, at which the sensor response reaches its maximum. In the present investigation, the sensor element based on pure Bi_2O_3 exhibited good response towards 50-ppm ethanol at an operating temperature of 300 ^{0}C as compared to other tested gases at the same temperature.

ISSN 2348 – 8034
Impact Factor- 5.070

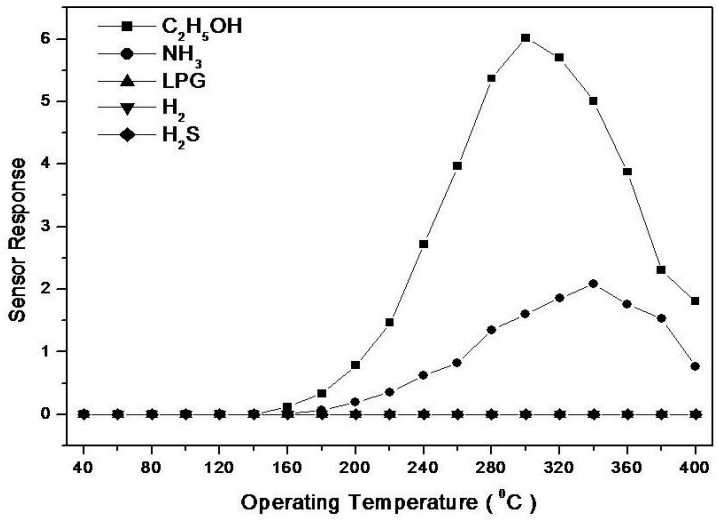

Fig. 4: Sensor response of pure Bi_2O_3 to different reducing gases as a function of operating temperature.

It should be noted that the changing trend in the resistance of the p-type semiconductor sensor with the concentration of the reducing gas was completely opposite to that of an n-type sensor, implying that their sensing mechanisms are different. The major charge carriers are holes and electrons for p-type and n-type semiconductors, respectively. Upon exposure to a reducing gas, the density of p-type charge carriers (positive holes) would decrease due to surface adsorption and chemical reaction between the gas and the oxygen adsorbates (electron acceptor), resulting in an increase of its resistance, which is opposite to what is seen with the n-type semiconductor gas sensors [27,28].

The adsorption–desorption of molecules at the sensor surface is the principle mechanism for gas detection. The surface Bi_3^+ ions act as donors, removing holes from the Bi_2O_3. The surface oxygen, O– or O_2–, forms a donor–acceptor complex with the surface of Bi3+, restoring holes in the valence band and increasing the conductivity. In the first place the adsorbed gaseous species at the bismuth oxide surface acts as an electron donor, changing Bi_4^+ to Bi_3^+ and removing holes from the Bi_2O_3 valence band. Ethanol reacts with the adsorbed oxygen and the resulting Bi_3^+ donors decrease the conductivity. Therefore, with reducing gas on this p-type sensor, the conductivity drops. Upon removal of reducing species or introduction of air or oxygen, the mechanism is reversed and the conductivity returns to its original state. When the semiconductor material is exposed to air, the atmospheric oxygen molecules are adsorbed on the sensitive material's surface in the four following forms [29-34]:

O_2 (gas) ↔ O_2 (ads) (3)
O_2 (ads) + e-↔ O_2- (ads) (4)
O_2- (ads) + e-↔ 2O- (ads) (5)
O- (ads) + e-↔ O_2- (ads) (6)

When exposed to C2H5OH, the interaction of C2H5OH with the surface chemisorbed O2-− takes place, thereby releasing electrons that recombine with holes to decrease the electrical conductance of the semiconductor. This causes the resistance to increase. The possibility of reaction on the Bi2O3-based sensor can be explained as

$C_2H_5OH + 6O– \rightarrow 3H_2O + 2CO_2 + 6e–$ (7)

The sensor response usually depends on the operating temperature and additive. There have been many reports showing that the gas-sensing properties of a semiconductor metal oxide based sensor are greatly affected by the additions of a noble metal or a metal oxide to the sensor element [35]. In particular, the dopant, besides acting as catalyst, can modify the electrical transport properties of the sensor by introducing new states in the band structure of the active materials. Besides this, the dopants can also modify: (a) The surface morphology of the material, which is a very important parameter, that influences the number of surface sites available for the chemical reactions to take place

between the sensor and the gas and (b) The size of the crystalline grains, which contribute in determining the electrical resistance of the material. Furthermore, oxide materials can contain Bronsted and Lewis acid/base sites. The acido-basic properties control the adsorption and desorption of the reactants and reaction products [36,37]. Acidic sites favour the adsorption of basic molecules and increase desorption of acidic products, and vice-versa [38].

IV. CONCLUSION

Nanocrystalline Bi_2O_3 powder samples were successfully prepared by ethyl alcohol mediated decomposition route with calcinations at 600 ^{0}C for 4 h. The prepared materials showed p-type semiconducting properties. Nanocrystline nature of the sample is confirmed from TEM and SAED characterization. Further, XRD and FT-IR spectra confirmed the formation of pure Bi_2O_3 phase. The sensors based on pure Bi_2O_3 showed good response to 50 ppm C_2H_5OH gas at 300 ^{0}C as compared with other tested reducing gases. The sensor based on pure Bi_2O_3 exhibited large response and good selectivity to ethanol, and good response-concentration linearity at 300 ^{0}C. The enhanced performance of pure Bi_2O_3 to 50 ppm C_2H_5OH may be attributed to the reduced crystallite size, presence of non-stiochiometric $Bi_2O_{2.33}$. The semiconducting nature of pure Bi_2O_3 is confirmed from the D.C Electrical conductivity measurements.

REFERENCES

1. *Hashim A.R Zalzala, Basheer Y. Muhson and Muhnad A. Ahmed (2012), Journal of Al-Nahrain University l.15 (1) 80-82*
2. *J.A. Switzer, M.G. Shumsky, E.W. Bohannan (1999), Science, **284** 293-296.*
3. *P. Shuk, H.D. Wiemhofer, U. Guth, W. Gopel, M.Greenblatt (1996), Solid State Ionics **89** 179-196*
4. *B.J. Yang, M.S. Mo, H.M. Hu, C. Li, X.G. Yang, Q.W. Li, Y.T. Qian (2004), Eur. J. Inorg. Chem. **9,** 1785- 1787.*
5. *C.C. Huang, L.C. Leu, K.Z. Fung, Electrochem. Solid-State Lett. **8** (2005) A204- A206.*
6. *H. Maeda, N. Tomita, H. Kumakura, K. Togano, Y. Tanaka (1995), Mater. Chem. Phys. **40** 298-302*
7. *X.L. Chen, W. Eysel (1996), J. Solid State Chem. **127** 128-130.*
8. *W.T. Dong, C.S. Zhu (2003), J. Phys. Chem. Solids, **64** 265-271*
9. *W.T. Dong, S.X. Wu, D.P. Chen, X.W. Jiang, C.S. Zhu (2000), Chem. Lett. **5,** 496-497*
10. *A. Cabot, A. Marsal, J. Arbiol, J.R. Morante (2004), Sens. Actuators B, **99,** 74-89.*
11. *O. Monnereau, L. Tortet, P. Llewellyn, F. Rouquerol, G. Vacquier (2003), Solid State Ionics, **157**, 163-169.*
12. *P. Maruthamuthu, K. Gurunathan, E. Subramanian (1994), Int. J. Hydrogen Energy, **19,** 889-893*
13. *K. Gurunathan (2004), Int. J. Hydrogen Energy, **29,** 933 - 940.*
14. *E.M. Levin, R.S. Roth (1964), J. Res. Natl. Bur. Stand. A, **68,** 189 –195*
15. *E.M. Levin, R.S. Roth (1964), J. Res. Natl. Bur. Stand. A, **68,** 197–206.*
16. *H.A. Harwig, A.G. Gerards (1979), Thermochim. Acta, **28,** 121-131*
17. *A.T. Liu, P. Kleinschmidt, R.W. Davidge (Eds.) (1986), Novel Ceramic Fabrication Process and Applications, **vol. 38**, Institute of Ceramics, Staffs, UK, , pp. 1–10.*
18. *N. Yamazoe, N. Miura, J. Tamaki, Advanced Materials, **93, II Vol. 15A**, p. 111-116.*
19. *R.K. Jha, R. Pasricha, V. Ravi (2005), Ceram. Int., **31,** 495-497.*
20. *L. Madler, S.E. Pratsinis (2002), J. Am. Ceram. Soc., **85** 1713-1718.*
21. *M.M. Patil, V.V. Deshpande, S.R. Dhage, V. Ravi (2005), Mater. Lett., **59,** 2523-2525*
22. *M. Anilkumar, R. Pasricha, V. Ravi (2005), Ceram. Int., **31,** 889-891*
23. *M.A. Matchett, M.Y. Chiang, W.E. Buhro (1990), Inorg. Chem., **29,** 358-360.*
24. *M.D.Wildberger, J.-D. Grunwaldt, M. Maciejewski, T. Mallat, A. Baiker (1998), Appl. Catal. A Gen., **175,** 11-19.*
25. *S.D. Kapse, F.C. Raghuwanshi, V.D. Kapse, D.R. Patil (2012), Current Applied Physics, **12,** 307-312.*
26. *N.T. G.enov, S. P. Yordanov (1996), Ceramic Sensors: Technology and Application, Technomic Pub. Lancaster, 134-145.*
27. *A. Gurlo, R. Riedel, Angew (2007). Chem. Int. Ed., **46,** 3826- 3848.*
28. *J. Zhang, J. Liu, Q. Peng, X. Wang, Y.D. Li (2006), Chem. Mater., **18**, 867- 871.*
29. *K.J. Albert, N.S. Lewis, C.L. Schauer, G.A. Sotzing, S.E. Stitzel, T.P. Vaid, D.R. Walt (2000), Chem. Rev., **100**, 2595-2626.*
30. *N. Barsan, D. Koziej, U. Weimar (2007), Sens. Actuators B, **121,** 18-35.*

31. *G. Sberveglieri, C. Baratto, E. Comini, G. Faglia, M. Ferroni, A. Ponzoni, A.Vomiero (2007), Sens. Actuators B,* ***121*** *208-213.*
32. *J.C. Belmonte, J. Manzano, J. Arbiol, A. Cirera, J. Puigcorbé, A. Vilà, N. Sabaté, I. Gràia, C. Cané, J.R. Morante (2006), Sens. Actuators B,* ***114,*** *881-892.*
33. *M. Egashira, Y. Shimizu, Y. Takao(1996), S. Sako, Sens. Actuators B,* ***35,*** *62-67.*
34. *K. Varghese, D. Gong, M. Paulose, K.G. Ong, C.A. Grimes (2003), Sens. Actuators B,* ***93*** *338-344.*
35. *J. Tamaki, T. Maekwa, S. Matsushima, N. Miura, N. Yamazoe (1990), Chem. Lett.,* ***19*** *477-480.*
36. *G. Centi, G. Golinelli, G. Busca (1990), J. Phys. Chem.,* ***94,*** *6813-6819.*
37. *P. Conception, A. Galli, J.M. Lopez Nieto, A. Dejoz, M.I. Vazquez (1996), Topics Catal.,* ***3,*** *451-460.*
J.C. Vedrine, J.M.M. Millet, J.-C. Volta (1996), Catalysis Today